North, A. C. T., Phillips, D. C., & Mathews, F. S. (1968) *Acta Crystallogr. A24*, 351–359.
Pearl, L. H. (1987) *FEBS Lett. 214*, 8–12.
Pearl, L. H., & Blundell, T. L. (1984) *FEBS Lett. 174*, 96–101.
Polgar, L. (1987) *FEBS Lett. 219*, 1–4.
Rae, A. D. (1965) *Acta Crystallogr. 19*, 683–684.
Rae, A. D., & Blake, A. B. (1966) *Acta Crystallogr. 20*, 586.
Read, R. J. (1986) *Acta Crystallogr. A42*, 140–149.
Rich, D. H., & Bernatowicz, M. S. (1982) *J. Med. Chem. 25*, 791–795.
Rich, D. H., & Salituro, F. G. (1983) *J. Med. Chem. 26*, 904–910.
Rich, D. H., Sun, E., & Singh, J. (1977) *Biochem. Biophys. Res. Commun. 74*, 762–767.
Rich, D. H., Sun, E. T. O., & Ulm, E. (1980) *J. Med. Chem. 23*, 27–33.
Richards, F. M., & Richmond, T. (1978) *J. Mol. Biol. 119*, 537–555.
Salituro, F. G., Agarwal, N., Hofmann, T., & Rich, D. H. (1987) *J. Med. Chem. 30*, 286–295.
Sibanda, B. L., Blundell, T. L., Hobart, P. M., Fogliano, M., Bindra, J. S., Dominy, B. W., & Chirgwin, J. M. (1984) *FEBS Lett. 174*, 102–111.
Sielecki, A. R., Hayakawa, K., Fujinaka, M., Murphy, M. E. P., Fraser, M., Muir, A. K., Carilli, C. T., Lewicki, J. A., Baxter, J. D., & James, M. N. G. (1989) *Science 243*, 1346–1351.
Singh, T. P., Haridas, M., Chauhan, V. S., & Kumar, A. (1987) *Biopolymers 26*, 819–829.
Suguna, K., Padlam, E. A., Smith, C. W., Carlson, W. D., & Davies, D. R. (1987) *Proc. Natl. Acad. Sci. U.S.A. 84*, 7009–7013.
Tang, J., James, M. N. G., Hsu, I. N., Jenkins, J. A., & Blundell, T. L. (1978) *Nature 271*, 618–621.
Thomas, K. A., Smith, G. M., Thomas, T. B., & Feldmann, R. J. (1982) *Proc. Natl. Acad. Sci. U.S.A. 79*, 4843–4847.
Tickle, I. J. (1985) in *Molecular replacement, proceedings of the Daresbury study weekend* (Machin, P., Ed.) DL/SCI/R23, pp 22–26, SERC, Daresbury Laboratory, U.K.
Umezawa, H., Aoyagi, T., Morishima, M., Matsuzaki, M., Hamada, M., & Takeuchi, T. (1970) *J. Antibiot. 23*, 259–261.
Webb, D. J., Cumming, A. M. M., Leckie, B. J., Lever, A. F., Morton, J. J., Robertson, J. I. S., Szelke, M., & Donovan, B. (1983) *Lancet ii*, 1486–1487.
Workman, R. J., & Burkitt, D. W. (1979) *Arch. Biochem. Biophys. 194*, 157–164.

Ruthenium–Iron Hybrid Hemoglobins as a Model for Partially Liganded Hemoglobin: Oxygen Equilibrium Curves and Resonance Raman Spectra†

Koichiro Ishimori,‡ Antonio Tsuneshige,§ Kiyohiro Imai,§ and Isao Morishima*,‡
Division of Molecular Engineering, Graduate School of Engineering, Kyoto University, Kyoto 606, Japan, and Department of Physicochemical Physiology, Medical School, Osaka University, Osaka 530, Japan
Received March 16, 1989; Revised Manuscript Received June 14, 1989

ABSTRACT: The structure and function of iron(II)–ruthenium(II) hybrid hemoglobins $\alpha(Ru\text{-}CO)_2\beta(Fe)_2$ and $\alpha(Fe)_2\beta(Ru\text{-}CO)_2$, which can serve as models for the intermediate species of the oxygenation step in native human adult hemoglobin, were investigated by measuring oxygen equilibrium curves and the Fe(II)–N_ϵ (His F8) stretching resonance Raman lines. The oxygen equilibrium properties indicated that these iron–ruthenium hybrid hemoglobins are good models for the half-liganded hemoglobin. The pH dependence of the oxygen binding properties and the resonance Raman line revealed that the quaternary and tertiary structural transition was induced by pH changes. When the pH was lowered, both the iron–ruthenium hybrid hemoglobins exhibited relatively higher cooperativity and a Raman line typical of normal deoxy structure, suggesting that their structure is stabilized at a "T-like" state. However, the oxygen affinity of $\alpha(Fe)_2\beta(Ru\text{-}CO)_2$ was lower than that of $\alpha(Ru\text{-}CO)_2\beta(Fe)_2$, and the transition to the "deoxy-type" Fe–N_ϵ stretching Raman line of $\alpha(Fe_2)\beta(Ru\text{-}CO)_2$ was completed at pH 7.4, while that of the complementary counterpart still remained in an "oxy-like" state under the same condition. These observations clearly indicate that the β-liganded hybrid has more "T"-state character than the α-liganded hybrid. In other words, the ligation to the α subunit induces more pronounced changes in the structure and function in Hb than the ligation to the β subunit. This feature agrees with our previous observations by NMR and sulfhydryl reactivity experiments. The present results are discussed in relation to the molecular mechanism of the cooperative stepwise oxygenation in native human adult hemoglobin.

In spite of a large number of investigations during the last several decades, the molecular mechanism of cooperative oxygen binding by hemoglobin (Hb)[1] is not yet fully understood. The cooperativity arises from the reversible transition between fully oxygenated and deoxygenated forms of human normal adult hemoglobin (Hb A), whose structures have been elucidated by X-ray crystallography [for example, see Baldwin (1980), Shaanan (1983), and Fermi et al. (1984)]. One of

† This work was supported by research grants from the Ministry of Education, Science and Culture of Japan (62220018 and 62790145).
* Author to whom correspondence should be addressed.
‡ Kyoto University.
§ Osaka University.

[1] Abbreviations: Hb A, human adult hemoglobin; NMR, nuclear magnetic resonance; Bis-Tris, [bis(2-hydroxyethyl)amino]tris(hydroxymethyl)methane; Tris, tris(hydroxymethyl)aminomethane; Ru-DPIXCO, ruthenium(II) carbonyldeuteroporphyrin; IHP, inositol hexakisphosphate.

0006-2960/89/0428-8603$01.50/0

the most challenging studies in current Hb research is to elucidate the structural change induced at each oxygenation step by observing the properties of the intermediate ligated species. Since at any given fractional saturation of molecular species of Hb A combining with zero to four ligands are in equilibria, it is not feasible to isolate them as stable intermediate compounds. This difficulty is not due to Hb A itself but rather to the use of O_2 as the ligand. The cooperative nature of oxygen binding further reduces the relative populations of intermediate species to small fractions in comparison with statistical populations.

Some efforts have been made to study the intermediate states of ligation, mainly focused on partially and symmetrically ligated hybrid hemoglobins. three types of symmetric Hbs have been extensively studied: (i) cyanomet valency hybrid Hbs, which contain two ferric hemes with cyanide at the α or β subunits (Brunori et al., 1970; Maeda et al., 1972; Bannerjee & Cassoly, 1969; Ogawa & Shulman, 1972; Cassoly & Gibson, 1972); (ii) the M-type Hb mutants, such as Hb M Milwaukee (Fung et al., 1977); and (iii) metal hybrid Hbs, such as iron–cobalt hybrid Hbs (Ikeda-Saito et al., 1977; Ikeda-Saito & Yonetani, 1980; Inubushi et al., 1983; Hofrichter et al., 1985), iron–zinc hybrid Hbs (Simolo et al., 1985), iron–manganese hybrid Hbs (Arnone et al., 1986), and iron–nickel hybrid Hbs (Shibayama et al., 1987).

Among these models, metal hybrid Hbs have certain advantages in that they are relatively stable and can be prepared in amounts enough to investigate their physicochemical and physiological properties. However, there has not been an appropriate, stable metalloporphyrin model for the oxy heme. Recently, ruthenium carbonylprophyrin was used as a model for the oxy heme (Ishimori & Morishima, 1988), and the structures of iron–ruthenium hybrid Hbs in which the α or β subunits contain ruthenium-substituted porphyrin with the other subunits having a deoxygenated iron porphyrin were investigated. Our previous studies (Ishimori & Morishima, 1988; K. Ishimori, R. Azumi, and I. Morishima, to be published) showed that ruthenium carbonylporphyrin is a novel model for the oxy heme, and a mechanism of structural propagation at oxygenation steps was proposed. In this paper, to gain further insight into the structural and functional properties of the intermediate species, we measured oxygen equilibrium curves and resonance Raman spectra of iron–ruthenium hybrid Hbs. On the basis of these observations, we attempted to describe the detailed mechanism of the R–T transition and cooperative oxygen binding in Hb A.

Materials and Methods

Preparation of Iron–Ruthenium Hybrid Hbs. Hemolysate was prepared by a standard method from whole blood samples obtained from a local blood bank. Hb A and its isolated chains were prepared in carbon monoxide form as described by Kilmartin et al. (Kilmartin & Rossi-Bernadi, 1971; Kilmartin et al., 1973) and Gerai et al. (1969). Ru-DPIXCO and iron–ruthenium hybrid Hbs were prepared as described previously (Ishimori & Morishima, 1988).

Measurement of O_2 Equilibrium Curves. Oxygen equilibrium curves were determined with an automatic oxygenation apparatus (Imai et al., 1970) equipped with an aerobic cell with variable light-path length (Imai & Yonetani, 1977), which was set at 20 mm in this study. The spectrophotometer used was a Cary Model 118C. The wavelength of the detection light was 564 nm. The temperature of the Hb sample was maintained constant within ±0.05 °C. The concentration of Hb samples as 60 μM on a metalloporphyrin basis. The pH conditions used in this study are listed in Table I. The buffers used were 0.05 M Bis-Tris for pHs 7.4, 6.9, and 6.4, and 0.05 M Tris for pH 7.9. These buffers contained 0.1 M Cl^- and were prepared from 0.05 M Bis-Tris or 0.05 M Tris solutions containing 0.1 M HCl by adjusting the pH with a concentrated NaOH solution at the same temperature as that for the oxygen equilibrium measurements (25 °C).

Table I: Oxygenation Parameters of Iron–Ruthenium Hybrid Hbs

	α(Ru-CO)$_2\beta$(Fe)$_2$				α(Fe)$_2\beta$(Ru-CO)$_2$			
pH	p_{50}[a]	n_{max}[b]	K_3[c]	K_4[c]	p_{50}	n_{max}	K_3	K_4
6.4	1.5	1.32	0.33	1.3	3.3	1.51	0.098	0.93
6.9	1.0	1.22	0.63	1.5	1.5	1.33	0.34	1.3
7.4	0.60	1.22	1.1	2.6	0.85	1.31	0.62	2.3
7.9	0.46	1.16	1.6	3.0	0.46	1.22	1.4	3.4

[a] Oxygen pressure (mmHg) at half-saturation (1 mmHg = 133.3 Pa). [b] Maximum slope of the Hill plot. [c] Equilibrium constant for the first (K_3) and second (K_4) oxygen molecules binding to the ferrous subunits of the hybrid Hbs ($mmHg^{-1}$).

The oxygen equilibrium curves of iron–ruthenium hybrid Hbs were analyzed according to the two-step oxygenated scheme (Imai, 1982). In this case, the third and fourth equilibrium constants for oxygen binding to the hybrid Hb K_3 and K_4 are expressed as

$$K_3K_4 = 1/p_{50}^2 \quad (1)$$

$$K_3/K_4 = [n_{max}/(2 - n_{max})]^2$$

where p_{50} is the partial oxygen pressure at 50% saturation and n_{max} is Hill's coefficient, obtained from the equilibrium curve.

Measurements of Resonance Raman Spectra. Raman scattering was excited by the 441.6-nm line of a He–Cd laser (Kinmon CDR 80 SG, Tokyo, Japan) and was recorded on a JEOL-400D Raman spectrometer. In order to avoid the photoreaction of ruthenium-substituted porphyrin, we used a spinning cell (1800 rpm) equipped with a system for evacuation. The sample volume was ~300 μL and the concentration was 50 μM. Measurements were carried out at 20 °C in the same buffer as used for the measurement of oxygen equilibrium curves. The frequency calibration of the spectrometer was performed with CCl_4 as a standard.

Results

Oxygen Equilibrium Curves for Iron–Ruthenium Hybrid Hbs. Figure 1 shows the oxygenation curves expressed by saturation vs log p plot (A) and their Hill plots (B) at pH 7.4 for Hb A and iron–ruthenium hybrid Hbs, α(Ru-CO)$_2\beta$(Fe)$_2$ and α(Fe)$_2\beta$(Ru-CO)$_2$, in which one type of subunits contains ruthenium-substituted porphyrin and the other bears native heme. Table I lists the oxygen affinity (p_{50}), Hill's constant (n_{max}), and the K_3 and K_4 values estimated by using eq 1. The O_2 equilibrium curves of Hb A and the iron–ruthenium hybrid Hbs converge at a high saturation range approaching a common line with a slope of unity, while the lower asymptotes for the hybrid Hbs diverge from that of Hb A. The O_2 equilibrium curve for α(Ru-CO)$_2\beta$(Fe)$_2$ shows low cooperativity with a Hill coefficient of 1.22. The estimated K_3 and K_4 values are plotted against pH in Figure 2A (closed circle and triangle, respectively). K_4 for α(Ru-CO)$_2\beta$(Fe)$_2$ is less pH dependent than K_3. The K_3 value for α(Ru-CO)$_2\beta$(Fe)$_2$ shows a pH dependence similar to that of K_3 for native Hb A, but some small difference was observed in the acidic region. The log p_{50} of α(Ru-CO)$_2\beta$(Fe)$_2$ is plotted as a function of pH in Figure 2B (closed circle). The oxygen affinity of α(Ru-CO)$_2\beta$(Fe)$_2$ is very high but significantly lower than that of the isolated α or β subunit (0.58 and 0.29 mmHg, respectively) (Ikeda-Saito et al., 1977). The slope of the log p_{50} vs pH plot

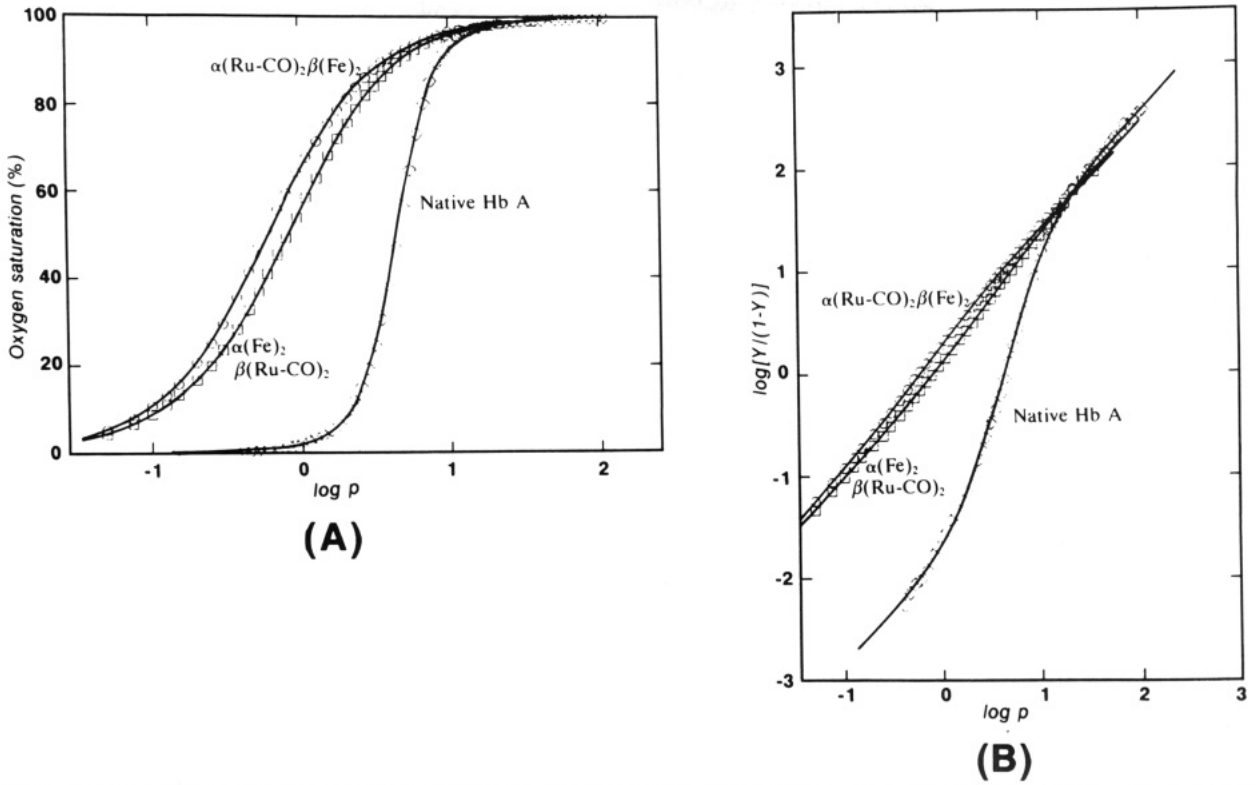

FIGURE 1: Oxygen equilibrium curves (A) and Hill plots (B) of native Hb A, $\alpha(\text{Ru-CO})_2\beta(\text{Fe})_2$, and $\alpha(\text{Fe})_2\beta(\text{Ru-CO})_2$. Y is the fractional oxygen saturation of ferrous suunits; p is the partial pressure of oxygen in mmHg. Conditions: 50 mM Bis-Tris with 100 mM chloride at pH 7.4; measurement temperature, 25 °C; heme concentration, 60 μM; wavelength of detection light, 564 nm.

is about −0.3 for $\alpha(\text{Ru-CO})_2\beta(\text{Fe})_2$ at pH 7.4, indicating that about 0.3 proton per native β subunit of $\alpha(\text{Ru-CO})_2\beta(\text{Fe})_2$ is released upon oxygenation.

The oxygen equilibrium curves of $\alpha(\text{Fe})_2\beta(\text{Ru-CO})_2$ at pH 7.4 are shown in Figure 1A. Incorporating ruthenium-substituted porphyrin into the β subunits also causes an increase in the oxygen affinity of the partner α subunits. However, the O_2 affinity of this hybrid Hb was considerably lower than that of $\alpha(\text{Ru-CO})_2\beta(\text{Fe})_2$. The former shows larger cooperativity, giving an n_{max} value of 1.3 at pH 7.4 and 1.5 at pH 6.4 compared to 1.2 at pH 7.4 and 1.3 at pH 6.4 for the latter. The pH dependence of the estimated K_3 and K_4 values was essentially the same as those of Hb A and the complementary hybrid Hb (Figure 2A). The Bohr effect was larger for $\alpha(\text{Fe})_2\beta(\text{Ru-CO})_2$ than for $\alpha(\text{Ru-CO})_2\beta(\text{Fe})_2$ (Figure 2B). The slope of the log p_{50} vs pH plot indicated that 0.5 proton was released upon the oxygenation of one α subunit, and this number is almost the same as that of native Hb A.

Resonance Raman Spectra of Iron–Ruthenium Hybrid Hbs. The excitation of Raman scattering at 441.6 nm selectively enhanced the Raman lines of the deoxy ferrous subunits within iron–ruthenium hybrid Hbs. In Figure 3A are shown the resonance Raman spectra of $\alpha(\text{Ru-CO})_2\beta(\text{Fe})_2$ at various pH values. At pH 7.4 with IHP, the resonance Raman line of the Fe–N_ϵ stretching in the β subunit was observed at 219 cm^{-1}, which is characteristic of the deoxy state as found for $\alpha(\text{Fe}^{III}\text{-CN}^-)_2\beta(\text{Fe})_2$ in the presence of IHP (Nagai & Kitagawa, 1980). Upon pH increases from 6.4 to 8.4, the Fe–N_ϵ stretching Raman line exhibited a frequency shift from 220 to 223 cm^{-1}. The Fe–N_ϵ stretching Raman line at 223 cm^{-1} corresponds to the oxy strcuture (Nagai & Kitagawa, 1980).

Figure 3B illustrates the resonance Raman spectra of the complementary hybrid $\alpha(\text{Fe})_2\beta(\text{Ru-CO})_2$. The Raman line of the Fe–N_ϵ stretching for the deoxygenated α subunit was observed in a lower wavenumber region than that for deoxy β subunit. In the presence of IHP at pH 7.4, $\alpha(\text{Fe})_2\beta(\text{Ru-CO})_2$ showed a Raman line at 206 cm^{-1}, corresponding to the deoxy structure of the α subunit (Nagai & Kitagawa, 1980; Ondrias et al., 1982). Contrary to $\alpha(\text{Ru-CO})_2\beta(\text{Fe})_2$, the Raman line for the α subunits in the absence of IHP was broad and sometimes showed a flattened peak. No significant frequency shift was observed upon pH increases from 6.4 to 7.4. At pH 8.4, the Raman line became slightly sharp and asymmetrical, resulting in a higher wavenumber shift to 217 cm^{-1}. Similar behavior was reported for iron–nickel hybrid Hbs (Shibayama et al., 1986). Such resonance Raman spectra can be interpreted in two ways, one assuming the existence of a single line having an intermediate frequency and the other assuming a composite of two lines at 206 and 220 cm^{-1}, which correspond to the deoxy and oxy structures of the α subunit, respectively. The observed peak wavenumbers of the Fe–N_ϵ stretching resonance Raman line are plotted against pH in Figure 4.

Discussion

pH Dependence of Oxygen Binding Properties and Structure of Iron–Ruthenium Hybrid Hbs. The K_3 and K_4 values for the two iron–ruthenium hybrid Hbs and their pH dependences are similar to those for native Hb A, indicating that Ru-DPIXCO is a good model for a permanent oxy heme. Thus, we can conclude that iron–ruthenium hybrid Hbs imitate half-liganded Hb in which the first and second oxygen molecules are already bound.

Although the two hybrid Hbs show very high oxygen affinities comparable to isolated chains, significant cooperativity (n_{max} = 1.2∼1.5) is observed (Table I). These observations imply that the two iron–ruthenium hybrid Hbs assume an "R-like" state which differs from the typical "R" state and has some "T"-state character. In an acidic region, relatively higher n_{max} and p_{50} values were observed (Figure 2A and Table I). These increases in n_{max} and p_{50} values suggest that the pH decrease causes some changes of the structure and function

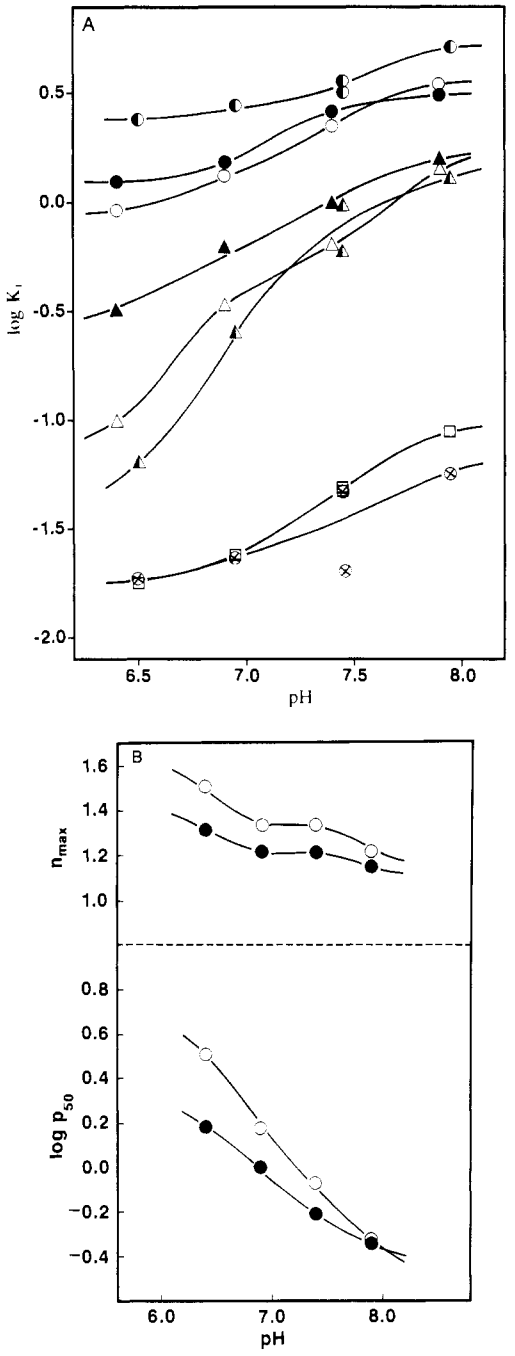

FIGURE 2: (A) pH dependence of logarithmic values of the equilibrium constants for the first [K_3, ▲ for α(Ru-CO)$_2\beta$(Fe)$_2$ and △ for α-(Fe)$_2\beta$(Ru-CO)$_2$] and second [K_4, ● for α(Ru-CO)$_2\beta$(Fe)$_2$ and ○ for α(Fe)$_2\beta$(Ru-CO)$_2$] oxygens binding to iron–ruthenium hybrid Hbs and for the first (K_1, ⊗), second (K_2, □), third (K_3, ▲), and fourth (K_4, ◐) oxygens binding to Hb A (Imai et al., 1977). (B) pH dependence of log p_{50} and n_{max} for iron–ruthenium hybrid Hbs [● for α(Ru-CO)$_2\beta$(Fe)$_2$ and ○ for α(Fe)$_2\beta$(Ru-CO)$_2$]. The parameter values were obtained from the O_2 equilibrium curves in Figure 1. Conditions: 50 mM Tris containing 100 mM Cl^- above pH 7.45 and 50 mM Bis-Tris containing 100 mM Cl^- below pH 7.45; heme concentration, 60 μM; temperature, 25 °C.

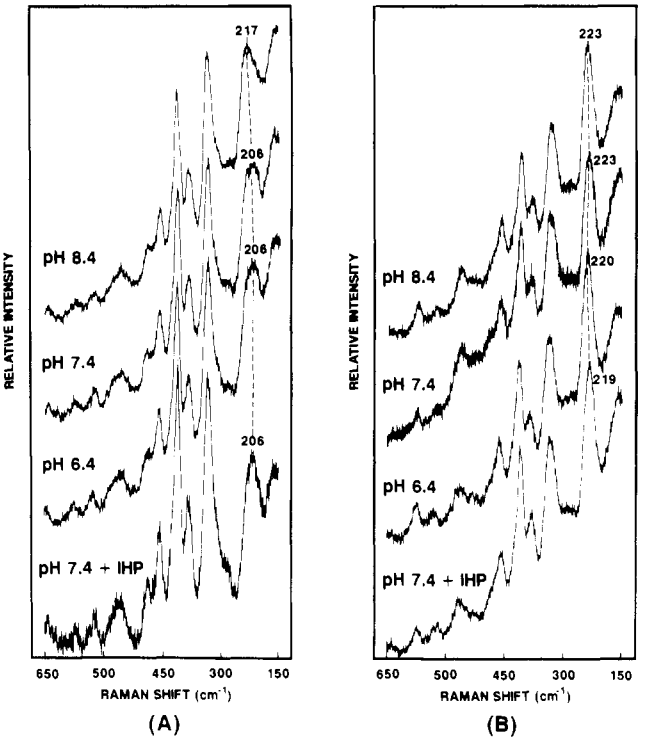

FIGURE 3: Resonance Raman spectra of deoxy α(Ru-CO)$_2\beta$(Fe)$_2$ (A) and α(Fe)$_2\beta$(Ru-CO)$_2$ (B) in 50 mM Tris or Bis-Tris with 100 mM chloride at various pH values in the absence of IHP and at pH 7.4 in the presence of 5 mM IHP. Measurements were carried out at 20 °C, excited at 441.6 nm. The spectra at pH 5.9, 6.9, 7.9, and 8.9 are not shown to avoid overcrowding.

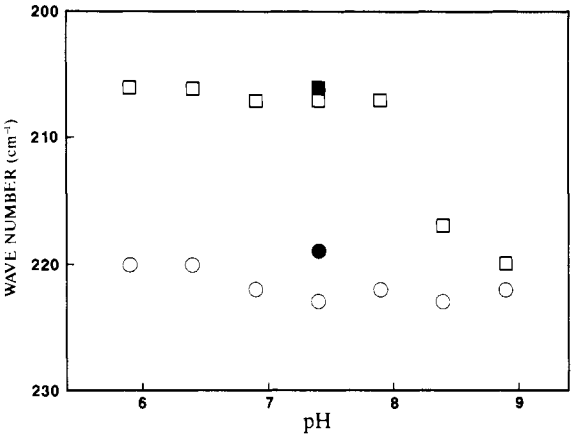

FIGURE 4: Plots of the peak wavenumber of Fe–N_ϵ stretching resonance Raman lines against pH for the two iron–ruthenium hybrid Hbs: (○) β(Fe) subunit of α(Ru-CO)$_2\beta$(Fe)$_2$; (□) α(Fe) subunit of α(Fe)$_2\beta$-(Ru-CO)$_2$. Filled symbols indicate the presence of IHP (5 mM).

of the iron–ruthenium hybrid Hbs toward the T state. The frequency of the Fe–N_ϵ stretching resonance Raman line has been shown to serve as a sensitive probe of the tertiary structure changes. Figure 4 clearly shows that the frequency of the Raman line is shifted to lower wavenumber as the pH is lowered, indicating that the strain of the Fe–N_ϵ bond is increased just as occurs in the transition from the R to T state (Nagai & Kitagawa, 1980). It is therefore concluded that the structural changes induced by the pH decrease affect the Fe–N_ϵ bond, lowering the oxygen binding affinity of the hybrids.

It should also be noted that oxygen binding properties of α(Fe)$_2\beta$(Ru-CO)$_2$ are more dependent on pH than those of the complementary hybrid and the oxygen affinity of the former is lower than that of the latter as shown in Fgiure 2 and Table I. In a previous paper (Ishimori & Morishima, 1988), we observed pH-dependent quaternary structure changes by means of NMR measurements of the hydrogen-bonded protons in α(Ru-CO)$_2\beta$(Fe)$_2$, but not in the complementary hybrid. In the NMR spectra of this hybrid, the proton resonance from the hydrogen bond between α42 Tyr

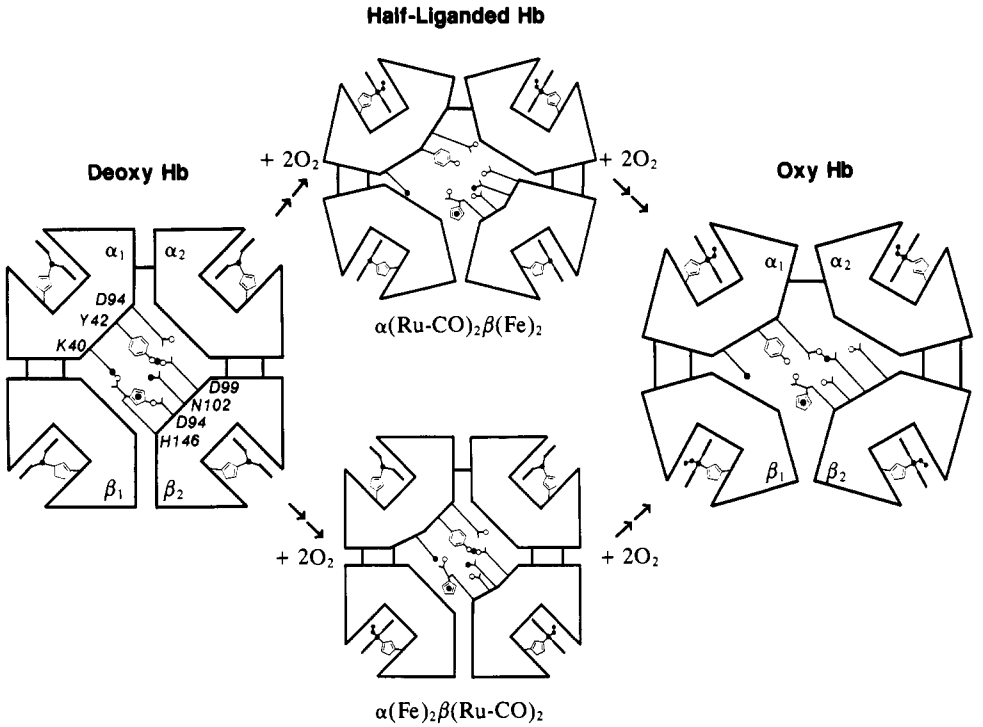

FIGURE 5: Schematic representation of the mechanism of the structural propagation in oxygenation (see text).

and β99 Asp, which is one of the T-state markers (Fung & Ho, 1975), lost its signal intensity, accompanied by the appearance of the R-state marker arising from the hydrogen bond between α94(G1) Asp and β102(G4) Asn (Takahashi et al., 1980). We concluded that the quaternary structure transition from the T-like state to the R-like state occurs by raising the pH. On the other hand, the complementary hybrid Hb α-$(Fe)_2\beta(Ru\text{-}CO)_2$ exhibited only small changes in the same pH region, and its NMR pattern indicated that its quaternary structure is fixed at T-like state even under alkaline conditions. Larger n_{max} values and Bohr effect for $\alpha(Fe)_2\beta(Ru\text{-}CO)_2$ are attributed to the T-state character in this hybrid. Therefore, the oxygenation in $\alpha(Fe)_2\beta(Ru\text{-}CO)_2$ accompanies more drastic structural changes than that in $\alpha(Ru\text{-}CO)_2\beta(Fe)_2$. On the other hand, the functional and structural properties of the α-liganded hybrid Hb exhibit less T-state character and are more similar to the isolated chains than those of the β-liganded hybrid. Therefore, the functional properties of the former hybrid are less influenced by pH perturbations like the isolated chains.

Another nonequivalence between the two hybrids is also manifested by their pH dependence of the $Fe\text{–}N_\epsilon$ stretching resonance Raman line. The wavenumber of the Raman line for $\alpha(Ru\text{-}CO)_2\beta(Fe)_2$ was shifted from that of the deoxy to the oxy state at pH 6.9, whereas in $\alpha(Fe)_2\beta(Ru\text{-}CO)_2$ this Raman line transition occurred at more alkaline pH. This implies that the T-like state in $\alpha(Fe)_2\beta(Ru\text{-}CO)_2$ is more stable than that of $\alpha(Ru\text{-}CO)_2\beta(Fe)_2$.

Such different pH dependences of structure and function between complementary hybrid Hbs were also found for iron–nickel hybrid Hbs (Shibayama et al., 1987). Shibayama et al. reported that $\alpha(Fe\text{-}CO)_2\beta(Ni)_2$ exhibits only slight NMR spectral changes upon pH decrease, while the NMR spectra of $\alpha(Ni)_2\beta(Fe\text{-}CO)_2$ show a drastic change associated with the rearrangement of the hydrogen bonds in the alkaline region due to the changes of the coordination state of the nickel-substituted porphyrin in the α subunit. The NMR pattern of $\alpha(Fe\text{-}CO)_2\beta(Ni)_2$ was characteristic of the R state, and the complementary hybrid exhibited the characteristic T-state markers in its NMR spectrum under acidic conditions. In this case, the R state was also more stable in the α-liganded hybrid than in the β-liganded one. Iron–zinc hybrid Hbs showed the same tendency (Simolo et al., 1985). It is thus likely that the ligand binding to the α subunit causes more extensive conformational and functional changes of Hb than to the β subunit.

However, the time-resolved resonance Raman spectra of the iron–cobalt hybrid showed that the contribution to the R-state stability from ligand binding in the β subunits is more significant than from ligand binding in the α subunits (Scott et al., 1983). A comparison of the signal intensity of the T-state markers between two complementary monoliganded asymmetric Fe–Co hybrids also indicated that the quaternary structure of $[\alpha(Fe\text{-}CO)\beta(Co)]_A[\alpha(Co)\beta(Co)]_CXL$ bears more T-state character than its complementary counterpart $[\alpha\text{-}(Co)\beta(Fe\text{-}CO)]_A[\alpha(Co)\beta(Co)]_CXL$ (Inubushi et al., 1986). They concluded that the binding of the first ligand to the β subunit induces more pronounced changes in the quaternary structure of Hb than the binding to the α subunit. Such discrepancy between iron–cobalt hybrid and iron–ruthenium hybrid Hbs could arise from the different modification of Hb. For example, the ligation state of the iron subunit in the iron–cobalt hybrid as a model for half-liganded Hb is different from that in the iron–ruthenium hybrid. Carbon monoxide is bound to the iron–heme in iron–cobalt hybrids, whereas the iron subunit in the iron–ruthenium hybrids is unliganded. It is also to be noted that the nonequivalence in structural changes induced by the heme substitution between the α and β subunits has been encountered for the many heme-substituted Hbs (Inubushi et al., 1983; Ishimori & Morishima, 1986). Since the present iron–ruthenium hybrid and the previous iron–cobalt hybrid studies showed that the α subunit substituted hybrid Hbs such as $\alpha(Co)_2\beta(Fe\text{-}CO)_2$ and $\alpha(Ru\text{-}CO)_2\beta(Fe)_2$ exhibit more R-state character than the β subunit substituted ones, the heme substitution of cobalt or ruthenium porphyrin for iron porphyrin in the α subunit may cause destabilization of the T state or stabilization of the R state. On the other hand, the β subunit hybrids $\alpha(Fe\text{-}CO)_2\beta(Co)_2$ and

Table II: Summary of Apparent Quaternary Structure States of Iron–Ruthenium Hybrid Hbs Determined by Different Structural Probes

	$\alpha(Ru\text{-}CO)_2\beta(Fe)_2$		$\alpha(Fe)_2\beta(Ru\text{-}CO)_2$		
	pH 7.4	pH 8.4	pH 7.4	pH 8.4	ref
α_1G1 Asp–β_2G4 Asn exchangeable proton	T	R (pH 8.7)	T	T	*a*
α_1C7 Tyr–β_2G1 Asp exchangeable proton	R	R	T	T	*a*
a_1C5 Lys–β_2HC3 His–β_2FG1 Asp salt bridge	R	R	intermediate	intermediate	*b*
Fe–N_ϵ stretching	R	R	T	R	*c*
p_{50} (mmHg)	0.60	0.46 (pH 7.9)	0.85	(pH 7.9)	*c*

[a] Ishimori & Morishima, 1988. [b] K. Ishimori, R. Azumi, and I. Morishima, to be published. [c] This work.

$\alpha(Fe)_2\beta(Ru\text{-}CO)_2$ may prefer the T state to the R state. More detailed investigation is needed to determine which hybrid model is suited to mimic the ligation intermediates of native Hb A.

Mechanism of Conformational Propagation upon Oxygenation. Ishimori and Morishima (1988) and Ishimori et al. (to be published) studied the quaternary and tertiary structures of iron–ruthenium hybrid Hbs by proton NMR spectra and sulfhydryl reactivity measurements. The results obtained by these studies are summarized in Table II. Inspection of this table shows that assignment of the conformational states in iron–ruthenium hybrid Hbs depends on the spectroscopic techniques used. Some probes indicate a T-like structure, while others claim a R-like structure. Therefore, the structure of the intermediate species during oxygenation cannot be described simply in terms of the "two-state" model, and the oxygenation-induced structural changes at various portions of the Hb molecule are not concerted. Table II indicates that the transition from the T to R state around the salt bridge at the $\alpha_1\beta_2$ interface, α_1 40(C5) Lys–β_2 146(HC3) His–β_2 94(FG1) Asp, precedes the structural changes associated with the hydrogen bonds located at the $\alpha_1\beta_2$ interface and with the Fe–N_ϵ stretching. The Fe–N_ϵ stretching mode could be converted from the T to R state by raising the pH, while the NMR spectra of the hydrogen bonds suggest that substantial rearrangement of the hydrogen bonds is required for the binding of the third oxygen molecule.

These findings allow us to propose a mechanism of the intersubunit conformational propagation upon oxygenation as schematically shown in Figure 5. When the two α subunits are ligated (half-liganded Hb in the figure) at neutral pH, the structural change around the heme iron affects the structure of α C helix, followed by the conformational change at the α 40(C5) Lys residue. This conformational change could induce a breakage of the salt ridge between β94(FG1) Asp and β146(HC3) His, the effect of which is then propagated onto the complementary subunits. The high oxygen affinity of the two hybrids and the high wavenumber shift of the Fe–N_ϵ stretching resonance Raman line suggest that the structure of the heme moiety of the β subunit is converted to the high oxygen affinity form with less strain on the Fe–N_ϵ bond. At this stage, the rearrangement of the hydrogen bonds occurs at the subunit interface with the cleavage of the T-state marker hydrogen bond but without formation of the R-state marker hydrogen bond. The complete transition from the T to the R state could not occur until binding of the third oxygen molecule to Hb. In the case of the ligation to the β subunit, the salt bridge is not completely broken (Ishimori et al., to be published) and the structural changes are partially propagated from the liganded β subunit to the unliganded α subunit. Thus, the unliganded α subunit in $\alpha(Fe)_2\beta(Ru\text{-}CO)_2$ bears more T-state character than the unliganded β subunit in the complementary hybrid. The present study suggests that the salt bridge between α_1 40(C5) Lys and β_2 146(HC3) His is one of the propagation of structural change paths from a liganded subunit to a unliganded subunit and the hydrogen bonds play a key role in the stablization of the high or low oxygen affinity form in Hb and are not contributed to the intersubunit structural propagation.

In summary, present studies on the iron–ruthenium hybrid Hbs have disclosed the structural and functional properties of the half-liganded Hbs. On the basis of these results, a plausible mechanism of the structural propagation during oxygenation was proposed. To gain further insight into the detailed mechanism, we plan to study asymmetric hybrid Hbs containing ruthenium-substituted porphyrin.

ACKNOWLEDGMENTS

We are grateful to Prof. T. Kitagawa and Dr. T. Ogura (Institute for Molecular Science) for resonance Raman spectra measurements.

REFERENCES

Arnone, A., Rogers, P., Blough, N. V., McGourty, J. L., & Hoffman, B. M. (1986) *J. Mol. Biol. 188*, 639–706.
Baldwin, J. M. (1980) *J. Mol. Biol. 136*, 103–128.
Banerjee, R., & Cassoyl, R. (1969) *J. Mol. Biol. 42*, 351–361.
Brunori, M., Amiconi, G., Antonini, E., Wyman, J., & Winterhalter, K. H. (1970) *J. Mol. Biol. 49*, 461–471.
Cassoly, R., & Gibson, Q. H. (1972) *J. Biol. Chem. 247*, 7332–7341.
Fermi, G., Perutz, M. F., Shaanan, B., & Fourme, R. (1984) *J. Mol. Biol. 175*, 159–174.
Fung, L. W.-M., & Ho, C. (1975) *Biochemistry 14*, 2526–2535.
Fung, L. W.-M., Minton, A. P., & Ho, C. (1976) *Proc. Natl. Acad. Sci. U.S.A. 73*, 1581–1585.
Fung, L. W.-M., Minton, A. P., Lindstrom, T. R., Pisciotta, A. V., & Ho, C. (1977) *Biochemistry 16*, 1452–1462.
Gerai, G., Parkhurst, L. J., & Gibson, Q. H. (1969) *J. Biol. Chem. 244*, 4664–4667.
Ikeda-Saito, M., & Yonetani, T. (1980) *J. Mol. Biol. 138*, 845–858.
Ikeda-Saito, M., Yamamoto, H., & Yonetani, T. (1977) *J. Biol. Chem. 252*, 8639–8644.
Imai, K. (1982) *Allosteric Effect in Haemoglobin*, Cambridge University Press, London.
Imai, K., & Yonetani, T. (1977) *Biochim. Biophys. Acta 490*, 164–170.
Imai, K., Morimoto, H., Kotani, M., Watari, H., Hirata, W., & Kuroda, M. (1970) *Biochim. Biophys. Acta 200*, 189–196.
Imai, K., Yonetani, T., & Ikeda-Saito, M. (1977) *J. Biol. Chem. 109*, 83–97.
Inubushi, T., Ikeda-Saito, M., & Yonetani, T. (1983) *Biochemistry 22*, 2904–2907.
Inubushi, T., D'Ambrosio, C., Ikeda-Saito, M., & Yonetani, T. (1986) *J. Am. Chem. Soc. 108*, 3799–3803.
Ishimori, K., & Morishima, I. (1986) *Biochemistry 25*, 4892–4898.
Ishimori, K., & Morishima, I. (1988) *Biochemistry 27*, 4060–4066.

Kilmartin, J. V., & Rossi-Bernardi, L. (1971) *Biochem. J. 124*, 31–45.
Kilmartin, J. V., Fogg, J., Luzzana, M., & Rossi-Bernardi, L. (1973) *J. Biol. Chem. 248*, 7039–7043.
Maeda, T., Imai, K., & Tyuma, I. (1972) *Biochemistry 11*, 3685–3689.
Nagai, K., & Kitagawa, T. (1980) *Proc. Natl. Acad. Sci. U.S.A. 77*, 2033–2037.
Ogawa, S., & Shulman, R. G. (1972) *J. Mol. Biol. 70*, 315–336.
Ondrias, M. R., Rousseau, D. L., Kitagawa, T., Ikeda-Saito, M., Inubushi, T., & Yonetani, T. (1982) *J. Biol. Chem. 257*, 8766–8770.
Scott, T. W., Friedman, J. M., Ikeda-Saito, M., & Yonetani, T. (1983) *FEBS Lett. 158*, 68–72.
Shaanan, B. (1983) *J. Mol. Biol. 171*, 31–59.
Shibayama, N., Morimoto, H., & Kitagawa, T. (1986) *J. Mol. Biol. 192*, 331–336.
Shibayama, N., Inubushi, T., Morimoto, H., & Yonetani, T. (1987) *Biochemistry 26*, 2194–2201.
Simolo, K., Stucky, G., Chen, S., Bacley, M., Scholes, C., & Mclendon, G. (1985) *J. Am. Chem. Soc. 107*, 2865–2872.
Takahashi, S., Lin, A. K.-A. C., & Ho, C. (1980) *Biochemistry 19*, 5196–5202.

Theoretical Study of the Contribution of Aromatic Side Chains to the Circular Dichroism of Basic Bovine Pancreatic Trypsin Inhibitor†

Mark C. Manning‡ and Robert W. Woody*
Department of Biochemistry, Colorado State University, Fort Collins, Colorado 80523
Received April 7, 1989

ABSTRACT: Circular dichroism (CD) spectroscopy is frequently employed to determine the secondary structure composition of a protein. However, this assumes that the far-UV region of the spectrum, which is used for these analyses, is due only to contributions from the polypeptide backbone. Basic bovine pancreatic trypsin inhibitor (BPTI) possesses an unusual far-UV CD spectrum, which has made such an analysis difficult. One possible reason for the discrepancy is that other chromophores, such as the aromatic side chains (four tyrosines, four phenylalanines), might be responsible. The CD spectrum of BPTI was calculated by employing a variation of the matrix method. Including only the peptide backbone gave poor agreement between theory and experiment. This was shown to be independent of the quality of the calculation performed. Subsequent inclusion of tyrosine contributions did little to improve the fit. However, further inclusion of the phenylalanine chromophores provided a good fit between the calculated and experimental far-UV spectrum. The important contributions arise from the cluster of aromatic amino acids formed by two tyrosines (Tyr^{21} and Tyr^{23}) and three phenylalanines (Phe^{22}, Phe^{4}, and Phe^{45}). Consideration of both types of side chains and the entire peptide backbone is essential to produce an accurate description of the CD curve. Overall, these results indicate that contributions from aromatic amino acids can significantly perturb the far-UV CD spectrum of a protein, making secondary structure analysis difficult. This is particularly true in systems like BPTI, with low amounts of α-helical structure and clusters of aromatic amino acids.

Recent developments have allowed a greater understanding of the mechanisms of protein folding and the determinants of protein conformation in solution. Basic bovine pancreatic trypsin inhibitor (BPTI)[1] has been a primary system for study in these areas. Its conformation has been extensively examined by nuclear magnetic resonance (NMR) (Snyder et al., 1975; Wagner, 1983; DeMarco et al., 1985; Wüthrich, 1986; Wagner et al., 1987a,b), circular dichroism (Kosen et al., 1981, 1983), and absorption (Kosen et al., 1980) spectroscopy. The role of disulfide bond formation in controlling the folding to the native conformation has been well documented (Creighton, 1984; Marks et al., 1987; States et al., 1987). In addition, BPTI has been the subject of molecular mechanics (Dunfield & Scheraga, 1980; Chou et al., 1985; Billeter et al., 1987) and molecular dynamics (Gelin & Karplus, 1975; McCammon et al., 1979; van Gunsteren et al., 1983) studies. All evidence indicates that BPTI adopts a relatively rigid, compact globular structure in solution similar to the conformation deduced by X-ray crystallography (Deisenhofer & Steigemann, 1975; Bode et al., 1984; Wlodawer et al., 1984, 1987a,b). Despite the wealth of data available on this protein, no detailed theoretical analysis of its circular dichroism (CD) has been published. Secondary structure estimates based upon the far-UV CD spectrum of BPTI have yielded poor results. The large fraction of aromatic residues (4 tyrosines, 4 phenylalanines, and no tryptophans out of 58 residues) suggests that aromatic side chains may make important contributions to both the near- and far-UV CD spectrum of BPTI.

Contributions from aromatic side chains to the CD of proteins and polypeptides have been recognized in both experimental and theoretical studies (Hooker & Schellman, 1970; Chen & Woody, 1971; Strickland, 1974; Strickland & Mercola, 1976; Strassburger et al., 1982). Such effects are

† Financial support for this work was provided by USPHS Grant GM-22994.
* Author to whom correspondence should be addressed.
‡ Present address: Department of Pharmaceutical Chemistry, The University of Kansas, Lawrence, KS 66045.

[1] Abbreviations: BPTI, basic bovine pancreatic trypsin inhibitor; CD, circular dichroism; NMR, nuclear magnetic resonance; UV, ultraviolet.

0006-2960/89/0428-8609$01.50/0